Office of Contract Administration 23-FEB-1999 12:56

PROJECT CLOSEOUT - NOTICE

Closeout Notice Date 23-FEB-1999

Project Number E-21-K25 Doch Id 48680

Center Number 10/24-6-R0971-0A0

Project Director GAYLORD, THOMAS

Project Unit ECE

Sponsor JET PROPULSION LAB/CALIFORNIA INST. OF TECH

Division Id 4874

Contract Number 961214 Contract Entity GTRC

Prime Contract Number

Title ELECTROMAGNETIC ANALYSIS & DESIGN OF QUANTUM WELL INFRARED PHOTODETECTOR...

Effective Completion Date 30-JAN-1999 (Performance) 30-JAN-1999 (Reports)

Closeout Action:	Y/N	Date Submitted
Final Invoice or Copy of Final Invoice	Y	
Final Report of Inventions and/or Subcontracts	Y	
Government Property Inventory and Related Certificate	Y	
Classified Material Certificate	N	
Release and Assignment	Y	
Other	N	

Comments

Distribution Required:	
Project Director/Principal Investigator	Y
Research Administrative Network	Y
Accounting	Y
Research Security Department	N
Reports Coordinator	Y
Research Property Team	Y
Supply Services Department/Procurement	Y
Georgia Tech Research Corporation	Y
Project File	Y

NOTE: Final Patent Questionnaire sent to PDPI

E-21-K25
#1

Modeling of Optical Coupling Structures for Quantum Well Infrared Photodetectors

Performed for the
Integrated Multispectral Atmospheric Sounder (IMAS) Program

IMAS QWIP Modeling Team:

Daniel Wilson, JPL Section 346
Andrea Borgioli, JPL Section 385
Thomas Cwik, JPL Section 385
Elias Glytsis, Georgia Institute of Technology
Thomas Gaylord, Georgia Institute of Technology

Contents:

I. Summary of Results

This section provides a high-level summary of the modeling results. It is meant to give the informed reader a quick overview of the conclusions gained from the IMAS QWIP modeling effort. For a more complete description, please see Secs. II-VIII.

A. *Infinite grating (normal and angled incidence)*

Coupling structure: an infinite-width binary grating. The goal was to optimize the grating period, depth, and fill factor for maximum QWIP coupling.

Modeling: Plane-wave incidence on one-dimensional infinite gratings was rigorously analyzed. The efficiencies of the diffracted orders were determined as functions of grating parameters, wavelength, and angle of incidence. A complete set of tools was developed for modeling 1D QWIP gratings, including the case of anisotropic absorption (component of electric field perpendicular to QW layers is absorbed). The development of simulation tools for 2D metal gratings is not complete.

Results:

- For normal incidence on a standard grating (period = 4.85 mm, depth = 1.28 mm, GaAs fill factor = 68%), enhancement over 45-degree incidence on no grating = 6.5 (non-absorbing model), = 4.2 (weak anisotropic absorbing model), = 2.0 (strong anisotropic absorbing model). The disparity in the results is due to the absorption and indicates that if the QWIP is strongly absorbing, then high grating-coupled to 45-degree enhancement ratios should not be expected.
- Determined that the QWIP grating is highly sensitive to angle of incidence. The standard grating only couples radiation within ±1.5 degrees from normal incidence. Increasing the grating period can widen the acceptance cone, but the peak coupling is reduced. This explains why experiments with microlenses over QWIPs did not work well.
- Determined that gold need not cover the grating sidewalls. Results with and without gold on the grating groove sidewalls were nearly identical.
- Determined the optimum period and fill factor to be 4.85 μm and 68% GaAs, respectively, for one-dimensional infinite gratings. These results and an approximate 2D grating analysis indicate that the current IMAS *two-dimensional* gratings may have a fill factor that is too small. The simulations identified 0.5 μm as the optimum depth, but this may be due to a long-range interaction that would not occur in finite QWIPs.

B. *Finite grating (normal and focused incidence)*

Coupling structure: a finite-width grating without mesa sidewalls. The aim was to determine the effects of finite grating size for normal plane-wave incidence and focused-beam incidence (from a microlens).

Modeling: Rigorously determined (a) microlens efficiency, (b) QWIP optical coupling for plane-wave and focused-wave incidence. Grating parameters including the depth and period were varied.

Results:

- Determined that a perfectly fabricated lens would focus ~87% of the incident light into a 15 μm wide region. This includes reflection losses at the air-GaAs interface. This is actually better than a flat air-GaAs interface because the surfaces of the lens approach the Brewster angle for total transmission of TM polarized radiation.

- Finite-width gratings showed less coupling than infinite gratings (coupling measured over same width in both cases). The greater coupling in the infinite gratings is due to high-angle waves originating outside of the measurement region. In finite structures, these waves do not exist.
- The optimum depth for the finite width grating is not the same as for the infinite grating, but ~68% fill factor is nearly optimum. The optimum depth for a 50 μm wide grating was ~0.8 μm.

C. Finite grating on mesa (normal and focused incidence)

Coupling structure: a microlens on the backside of the wafer to focus light onto a small QWIP mesa with a grating. The reduction in QWIP area would decrease the dark current and increase the signal-to-noise ratio. For this to work, the lens must be efficient and the grating on the small mesa must couple the light efficiently into the QWIP.

Modeling: Simulated radiation focused to gratings on finite mesas to determine the optical coupling efficiency.

Results:

- The optical coupling efficiency of focused light incident on a 20 μm mesa+grating is approximately 40% compared to unfocused light (no lens) incident on a 50 μm mesa+grating (λ = 15 μm). Multiple grating depths and fill factors were simulated and no substantial improvement was found.

D. Slotted QWIP (no microlens)

Coupling structure: standard mesa and grating with slots of QWIP material removed. The removal of QWIP material reduces dark current. The goal was to find structural parameters that yield strong optical coupling.

Modeling: Simulated the slotted QWIP structure using the infinite grating, anisotropic absorption model.

Results:

- Slotted QWIP can achieve higher absorption than standard grating on QWIP.
- Functional form of absorption as a function of wavelength indicates that resonance is more cavity-like than grating-like.
- Initial understanding of the structure is that the pillars act as micro-cavities, open on one end, closed on the other with a scattering tooth.

II. Introduction

This report describes a modeling effort that was aimed at enhancing the performance of quantum-well infrared detectors (QWIPs).[1] Specifically, the goal was to optimize the optical coupling efficiency of the IMAS detectors. Due to quantum mechanical selection rules,[2] a QWIP only absorbs light that has its electric field polarized perpendicular to the quantum well layers. Because the incoming light usually enters the detector at normal incidence (0 degrees from the surface normal), the polarization is parallel to the layers and is not absorbed. To overcome this problem, QWIP detectors usually employ a reflective corrugated surface that scatters the light at high angles as shown in Fig. 1. This scattered light has a component of its electric field vector perpendicular to the quantum well layers and can be absorbed. The corrugated surface can take many forms: it can be a periodic structure (grating)[3,4] that diffracts light into well-defined angles, or a random surface that scatters light into a broad range of angles. Grating reflectors typically exhibit high diffraction efficiency over a narrow wavelength range, whereas random reflectors have lower peak efficiency but are more broadband. Because the IMAS detector only needs to operate over a narrow wavelength range (14.7 – 15.4 μm), a grating reflector holds the most promise for high efficiency optical coupling. Therefore the reflectors considered in this project were either periodic or truncated periodic structures.

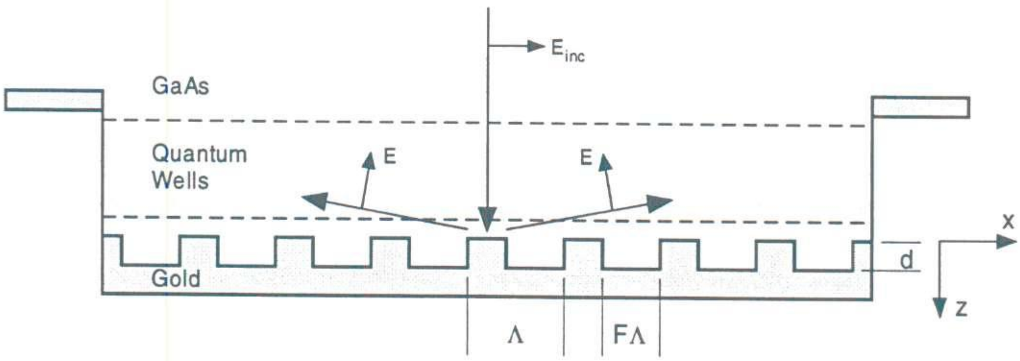

Figure 1. QWIP mesa with grating reflector. For the standard grating, $\Lambda = 4.85$ μm, $F = 68\%$, $d = 1.28$ μm, QW stack thickness = 3.33 μm, and grating-QW separation = 0.45 μm.

In addition to efficiently converting the polarization of the incoming light, it would be desirable to reduce the active area of the QWIP. This would reduce the dark current and hence increase the signal-to-noise ratio. Implicit in this argument is that the reduced-area QWIP must absorb the same amount of optical power as the standard QWIP. To achieve this, there must be a means of concentrating the light onto the smaller QWIP. The approach that was proposed for the IMAS program was to use a microlens on the opposite side of the QWIP wafer as shown in Fig. 2. However, preliminary experiments showed that the absorption of a grating-coupled QWIP was lower than expected when a microlens was used. Another approach for reducing the active area is to etch the corrugations all the way through the quantum well layers.[5,6] Several other QWIP groups have reported these types of structures, and a novel slotted QWIP is being considered in this program. In an effort to understand the poor performance of the microlens experiment and to potentially improve the performance, this modeling task was initiated.

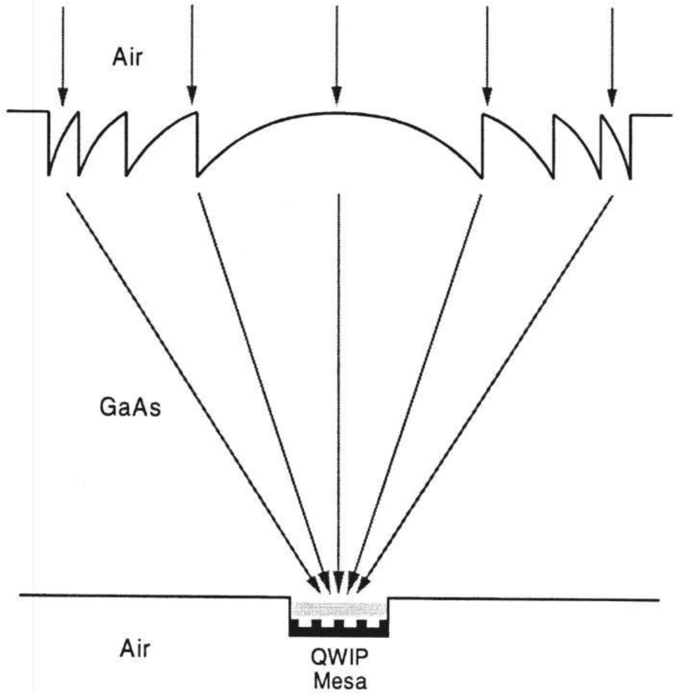

Figure 2. Lenslet focusing to reduced-area QWIP Mesa

In the following sections, the electromagnetic simulation techniques are briefly described and a variety of light coupling structures are quantitatively evaluated. Section III describes the modeling tools, Sec. IV describes infinite grating structures, Sec. V describes finite gratings without mesas, Sec. VI describes small-mesas with gratings, and Sec. VII describes a slotted QWIP structure.

III. Modeling tools

Modeling QWIP optical coupling structures is a significant challenge. First, because high-angle scattering is desired, the surfaces must have feature sizes very nearly equal to the wavelength. This rules out the possibility of using simple scalar diffraction models to calculate the scattered fields. Second, some of the structures of interest (small QWIP mesas) cannot be considered to be periodic because too few grating periods are present and the mesa walls influence of the scattering. For these structures, periodic electromagnetic models cannot be used. To handle the various structures, three types of electromagnetic modeling tools were used.

A. Rigorous Coupled-Wave Analysis (RCWA)

RCWA accurately calculates diffraction from *periodic structures* composed of arbitrary materials (including anisotropic).[7-11] In RCWA the grating permittivity is expanded as a Fourier series and the electromagnetic fields inside the grating region are expanded as a sum of spatial harmonics. These expansions are substituted into Maxwell's equations and a system of coupled equations for the harmonic amplitudes results. Another set of equations is derived from the boundary conditions at the input and output interfaces. Solving all the equations simultaneously yields the amplitudes of the diffracted orders in the input and output regions as well as the amplitudes of the spatial harmonics inside the grating. Because Maxwell's equations are being solved directly and all electric and magnetic field components are considered (E_x, E_y, E_z, H_x, H_y, H_z), the technique can handle isotropic and anisotropic materials.

During this project, RCWA was implemented in Matlab (a mathematical simulation / visualization environment that is available for many platforms). The code developed can treat multiple-layer periodic structures that may have multiple refractive indices within each layer. The grating parameters (period, depth, fill factor) can be easily varied and plots of the QWIP optical coupling as a function of the grating parameter(s) can be generated. The *onc-dimensional (1D)* grating code can treat the polarization required for QWIP simulations: transverse-magnetic (TM) polarization (magnetic field perpendicular to the plane of incidence), as well as transverse-electric (TE) polarization and conical polarization (arbitrary three-dimensional angle of incidence where all electric and magnetic field components are coupled). This 1D grating code is very efficient, taking on the order of several seconds to simulate each grating configuration. A code for treating arbitrary incidence on *two-dimensional (2D) dielectric* gratings has also been implemented and validated, but because of the increased computational cost of simulating 2D structures, it does not work well for 2D metallic gratings (too many diffraction orders are required). When an efficient 2D grating metallic grating solver is developed, it can easily be incorporated into the modular Matlab QWIP simulation tool.

B. Boundary Element Method (BEM)

BEM accurately calculates scattering from *arbitrary structures* composed of two isotropic materials.[12-14] It uses a Green's function formulation to calculate the fields on the boundary between the two materials. Once the boundary fields are determined, the fields anywhere in space can be calculated by evaluating an integral expression. Variation of the structure being considered requires calculating a new boundary polygon, specifying the incident field at points on the boundary, and recalculating the scattered fields. BEM's capability of treating non-periodic structures allows simulation of finite beams incident on finite-width gratings. However, BEM is much more computationally expensive than RCWA, so investigating a large parameter space is more time consuming.

C. *Finite Element Method (FEM)*

FEM also accurately calculates scattering from *arbitrary structures*, but it can handle any number of isotropic material regions. It solves equations derived from a variational formulation of the electromagnetic wave equation. The structure to be simulated is meshed into triangular elements that are small compared to the wavelength. Using the known values of the incident field on the perimeter of the simulation region, the fields in the interior are found. The FEM code implemented at JPL is an efficient *hybrid* FEM-BEM code that uses a BEM formulation on the perimeter to allow waves to exit the simulation region without reflection.[15] In FEM, if the grating structure is varied, then the problem must be re-meshed. This is inconvenient, but there are efficient, programmable, commercial mesh generators that allow relatively easy variation of grating parameters. Like BEM, FEM is computationally expensive compared to RCWA, but it allows simulations of finite beams incident on finite QWIP mesas, including the sidewalls.

D. *Merit functions*

Ideally, the modeling tools would give results that could be directly compared to experimental quantities such as responsivity. Because of the complicated electron transport in QWIPs, however, it is much more convenient to define merit functions that focus solely on the optical coupling. Two such merit functions were used in this project:

1. Field magnitude squared

The electromagnetic modeling tools calculate the fields throughout the quantum well region of the QWIP. The field component that gets absorbed is E_z, so a positive quantity that indicates the strength of this field component inside the quantum wells is

$$f_{merit} = \iint_{QW} |E_z|^2 \, dxdz \tag{1}$$

where the integral is taken over the quantum well area. For the case of infinite gratings, the width of the integration region is taken to be 50 μm. For all simulations, the incident field was a plane wave having an electric field strength E_0 = 1 V/μm inside the GaAs. For a *z*-polarized plane wave propagating in the *x*-direction, the merit function would be (width=50 μm)(height=3.33 μm)($|E_z|^2$=1 $V^2/\mu m^2$) = 166 V^2.

2. Anisotropic absorption

In the RCWA equations, all the field components are included and thus anisotropic media can be treated. This allows for a more accurate representation of the QW material. The refractive indices for E_x and E_z can be different: $n_x = 3.1$, $n_z = 3.1 - j(\alpha_z\lambda/4\pi)$, where α_z is the intensity absorption coefficient for z-polarized, x-propagating light. Because the real parts of the *x* and *z* indices are assumed equal, there is no birefringence to complicate the analysis. Although $\alpha_z(\lambda)$ is not yet known for the IMAS QWIP material, different levels of absorption can be included to determine its effect. The merit function when anisotropic absorption is included is simply the fraction of power absorbed. Because the gold absorbs some power, the QW absorption can be found from the difference of the total absorption and the gold absorption. Currently this anisotropic absorption model is implemented in RCWA only, so only periodic structures can be analyzed in this manner. In BEM and FEM, anisotropic absorption would be difficult to include because only the magnetic field perpendicular to the plane of incidence (the page) is included in the electromagnetic equations (E_x and E_z are determined from H_y using Maxwell's curl equations).

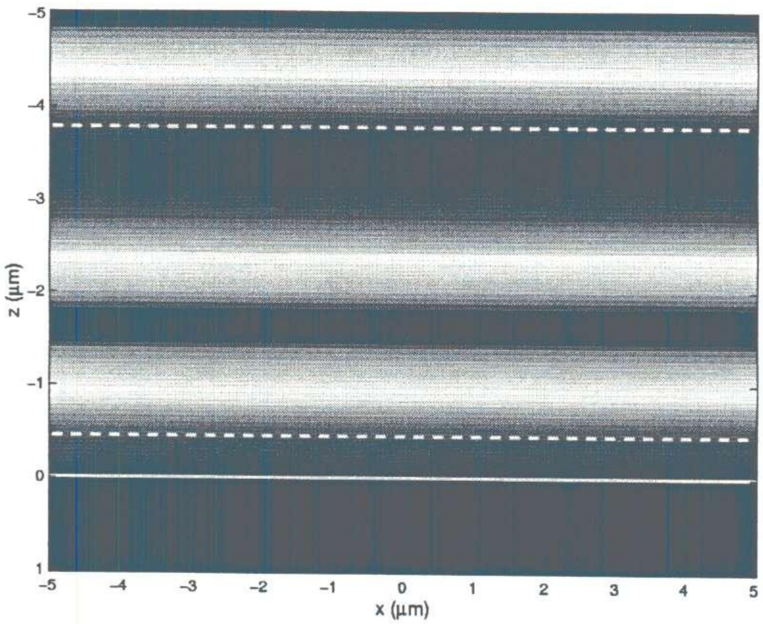

Figure 3. Electric field component perpendicular to quantum well layers (E_z) due to a 15 μm plane wave incident at 45 degrees on a planar GaAs/gold interface at z = 0 (solid line). Colormap: increasing field from blue to red, dashed lines indicate extent of quantum well stack.

B. Normal incidence on standard grating

Figure 4 shows a diagram of what will be termed the standard grating. This grating represents a one-dimensional slice through the two-dimensional grating that is currently being used for IMAS QWIP devices. The parameters of the standard grating are period Λ = 4.85 μm, depth d = 1.28 μm, and fill factor F = 0.68 (GaAs). In all simulations, the refractive indices of GaAs and gold are assumed to be 3.1 and 11.5 – j67.5, respectively. Figure 5 shows the diffraction efficiencies for two types of gold coatings: thick (filling in the entire groove), and thin (a 2000 Å layer that does not coat the sidewalls, they are open to air). Note that the ±1 orders cut off just above 15 μm, but the efficiencies below 15 μm are remarkably similar for the thick and thin coatings. Above 15 μm, the zeroth order leaks through the thin coating, but this is of no consequence for QWIPs. Figure 6 shows the merit function for the two gold coatings. The left axis shows the raw merit function and the right axis shows the merit functions divided by the 45-degree merit function. The merit functions of both types of gold coatings are sharply peaked at 15 μm (near cutoff), and have very nearly the same magnitude. Hence *the issue of coating the sidewalls of the grating grooves with gold should not be a concern during fabrication.* At wavelengths below 15 μm, both the +1 and –1 orders are propagating with high efficiency, but the diffraction angles are smaller than near cut off so the merit function drops off. At wavelengths above 15 μm, both the +1 and –1 orders are cut off, and the QWIP response is due to the evanescent fields that decay into the QW region.

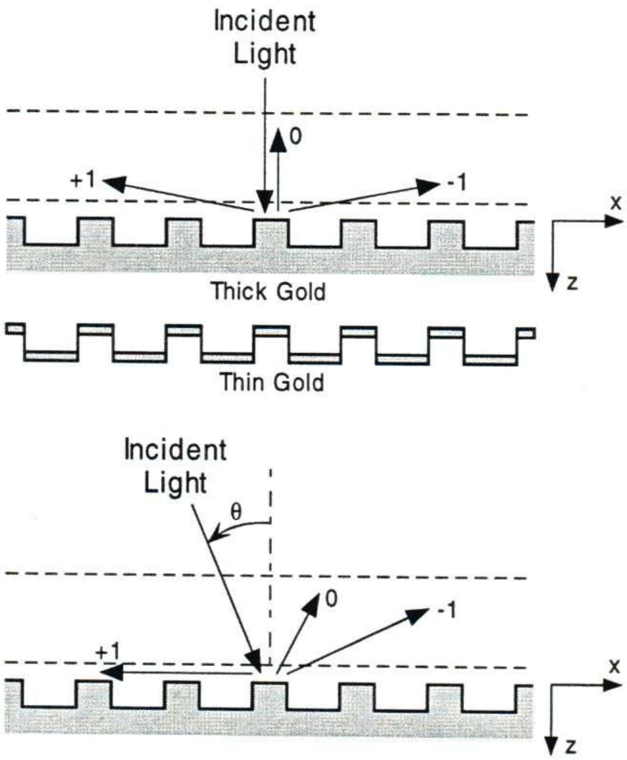

Figure 4. Standard infinite grating configuration showing thick gold, thin gold, and angled incidence. For the standard grating, $\Lambda = 4.85$ μm, F = 68%, d = 1.28 μm, QW stack thickness = 3.33 μm, and grating-QW separation = 0.45 μm.

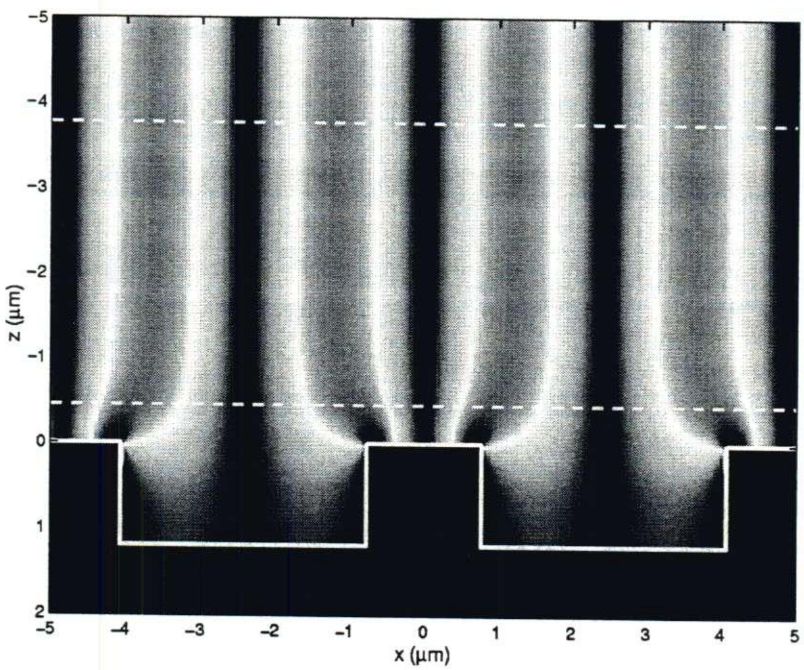

Figure 5. Electric field component perpendicular to quantum well layers (E_z) due to a 15 μm plane wave at normal incidence on a standard grating.

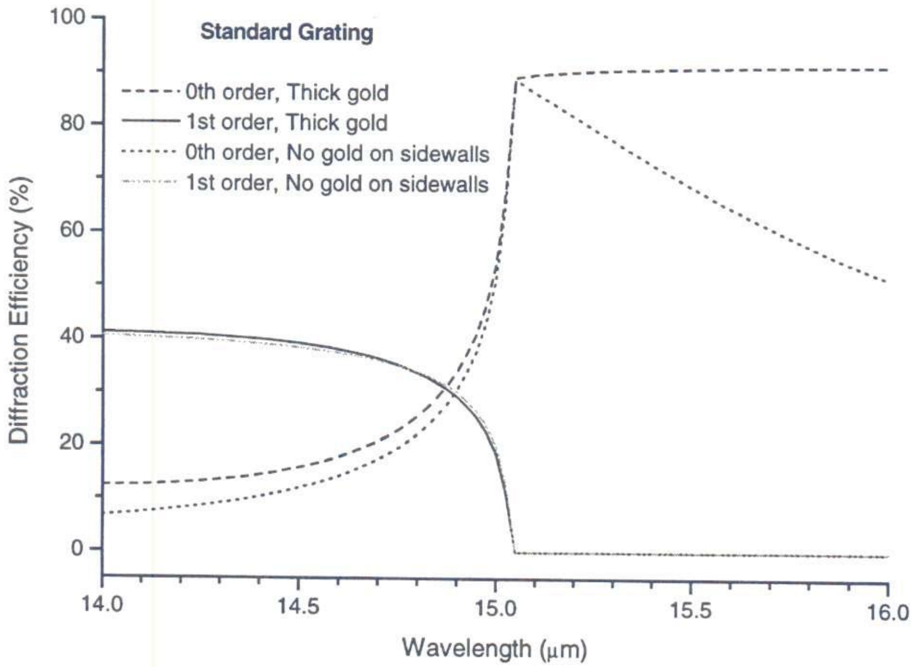

Figure 6. Diffraction efficiencies of the 0^{th} and 1^{st} orders for normal incidence on the standard QWIP grating coated with thick gold and thin gold.

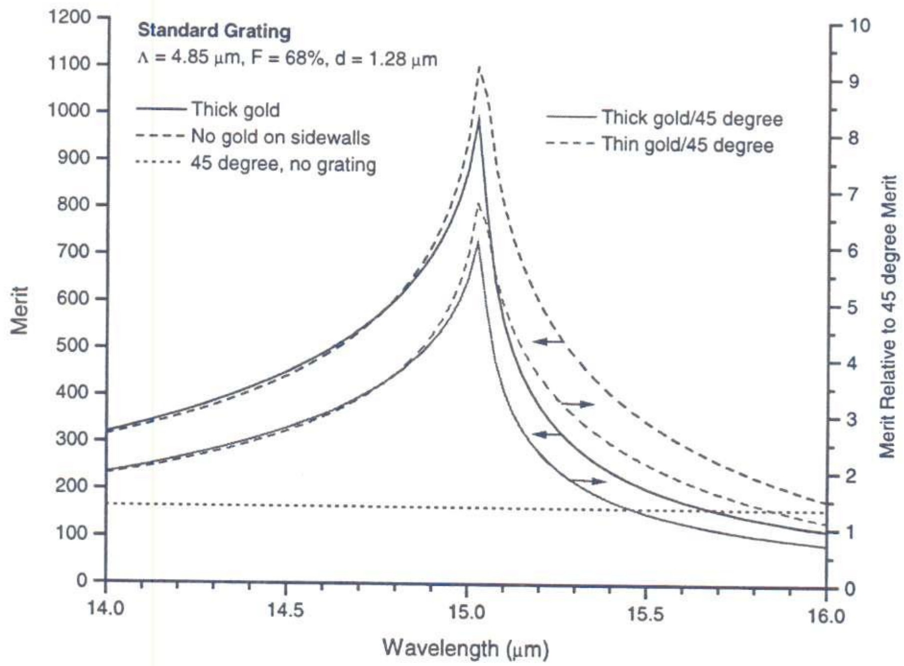

Figure 7. Field-magnitude squared merit function for the thick gold and thin gold standard grating at normal incidence. Left axis: merit function value. Right axis: merit function relative to the 45 degree no-grating merit function.

In the above-described simulation, the QW region was considered non-absorbing. It is interesting to consider the effect of anisotropic absorption on the results. Figure 8 shows the total absorption for two levels of QWIP absorption coefficient. In the case of low absorption (α_z = 84 cm^{-1}), the QW absorption curve has a shape similar to the non-absorbing case shown in Fig. 6. For 10X higher absorption (α_z = 840 cm^{-1}), however, the absorption below 15 μm drops off less rapidly than in Fig. 7 and the peak relative to the 45-degree case is only ~2 as opposed to ~4. It is apparent that the field-squared merit function may overestimate the enhancement of the grating-coupled QWIP relative to the 45-degree case, but it is still useful for optimizing the grating parameters. This also indicates that *if the QWIP has been designed for high absorption, then it is unrealistic to expect large grating-coupled to 45-degree enhancement ratios.*

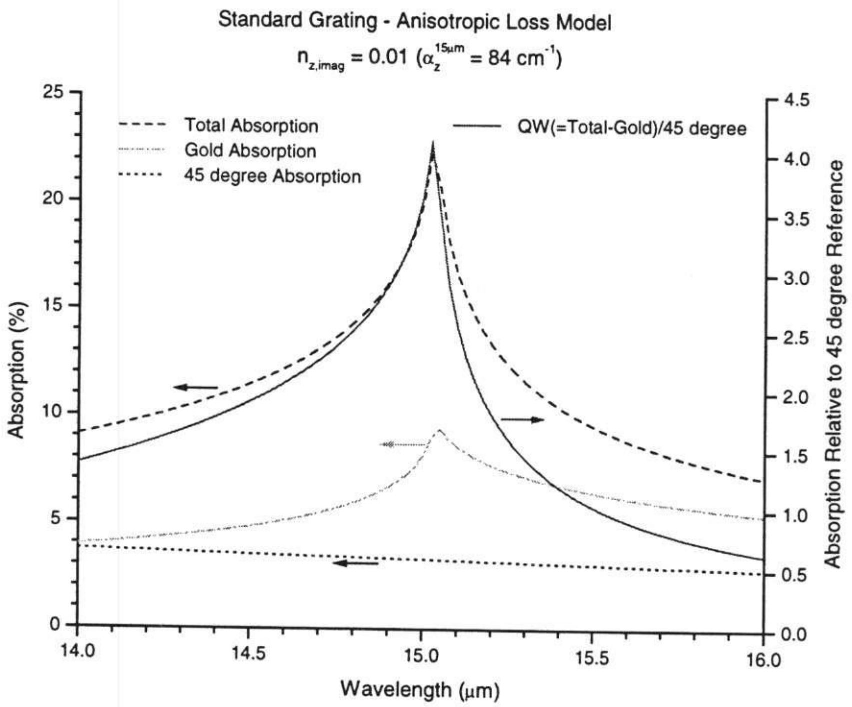

(a)

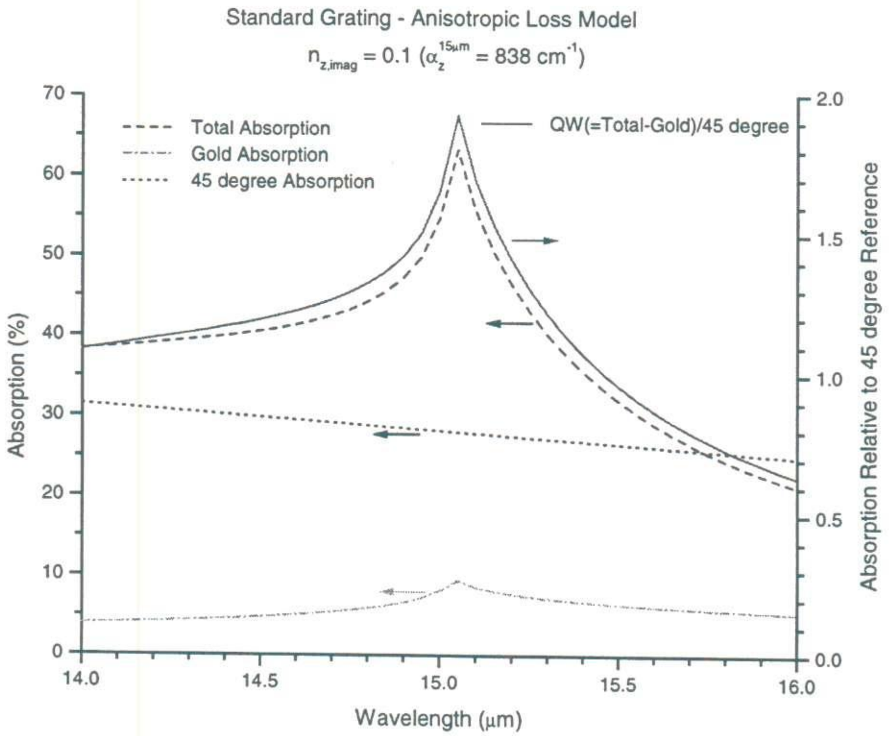

(b)

Figure 8. Results for normal incidence on standard grating using the anisotropic absorption model. (a) low absorption, (b) high absorption. Left axis: percentage of incident power absorbed, right axis: absorption in QW layers normalized by the absorption of 45 degree incidence with no grating.

C. Angular sensitivity of standard grating.

One of the main goals of this modeling task was to understand the angular sensitivity of the optical coupling. The proposed IMAS microlens was 50 μm wide and had a focal length of 90 μm. Hence the ray angles range from –15 to +15 degrees. The focused field from the lens is not a plane wave, but it can be Fourier decomposed into an angular spectrum of plane waves, so RCWA can be used. Figure 9 shows the diffraction angles, order efficiencies, and the merit function of the standard grating to this range of incident angles. As the incident angle is increased, the angle of the –1 order decreases and the +1 order eventually cuts off. At $\lambda = 15$ μm, the coupling is strongly peaked around normal incidence even though the diffraction efficiencies are not well optimized (the zeroth order is not minimized). At a shorter wavelength of 14.5 μm, the period to wavelength ratio is larger, allowing both the +1 and –1 orders to continue to propagate up to a few degrees off normal as shown in Figure 9(c). This broadens the angular response, but because the angles of the diffracted orders are smaller, they do not couple as effectively into the QWIP and the peak response is reduced. At 15.5 μm, the coupling at normal incidence is purely due to evanescent fields up to ±5 degrees where either the +1 or -1 order begins to propagate. For a given lens, there is certainly an optimum grating period that maximizes the integrated product of the focused-field angular spectrum and the grating angular response. However, *it is highly unlikely that a lens-grating combination will achieve the same responsivity as a grating optimized for plane wave illumination.* Further evidence of this will be given in Secs. V and VI.

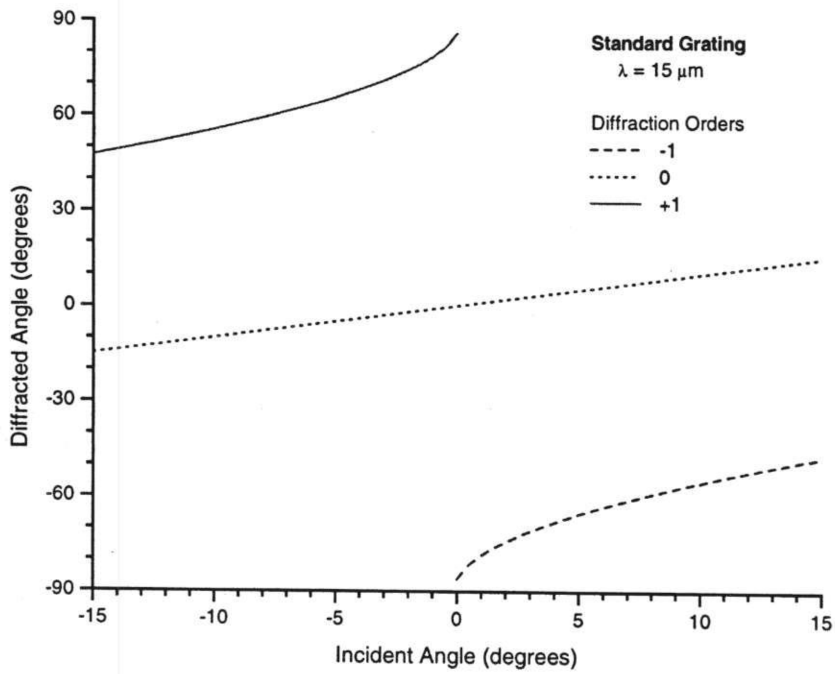
Standard Grating
λ = 15 μm
Diffraction Orders
-1
0
+1
Diffracted Angle (degrees)
Incident Angle (degrees)
90
60
30
0
-30
-60
-90
-15
-10
-5
0
5
10
15

(a)

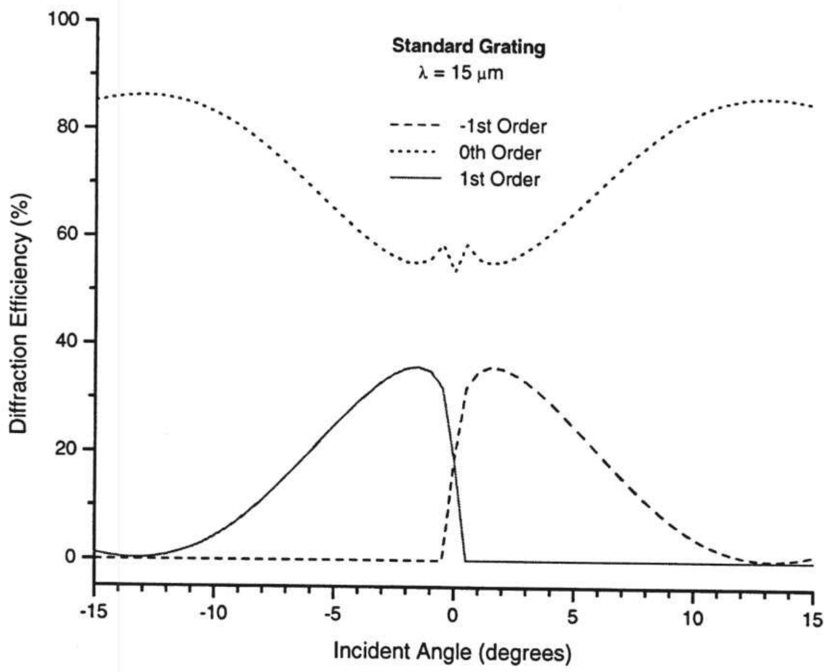
Standard Grating
λ = 15 μm
-1st Order
0th Order
1st Order
Diffraction Efficiency (%)
Incident Angle (degrees)
100
80
60
40
20
0
-15
-10
-5
0
5
10
15

(b)

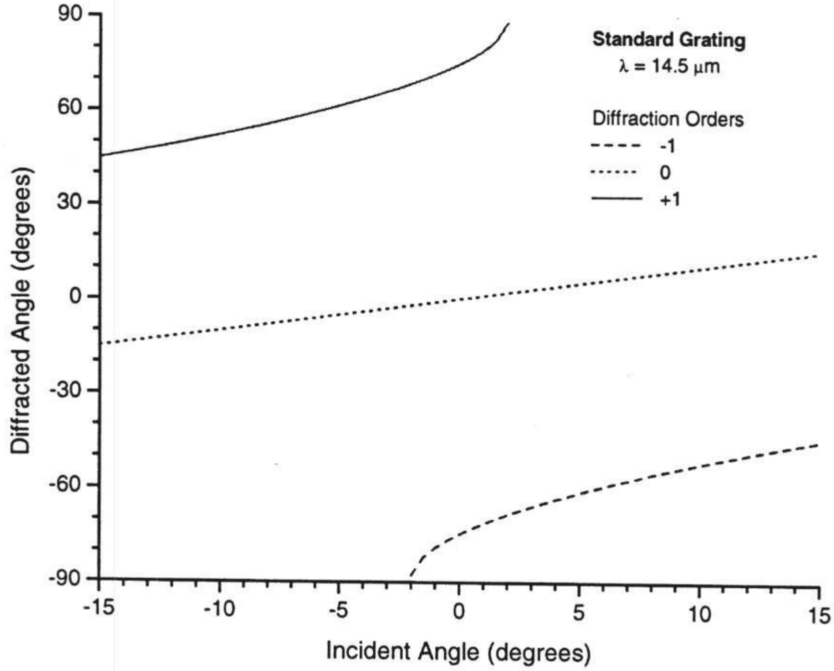
Standard Grating
λ = 14.5 μm
Diffraction Orders
-1
0
+1
Diffracted Angle (degrees)
Incident Angle (degrees)
90
60
30
0
-30
-60
-90
-15
-10
-5
0
5
10
15

(c)

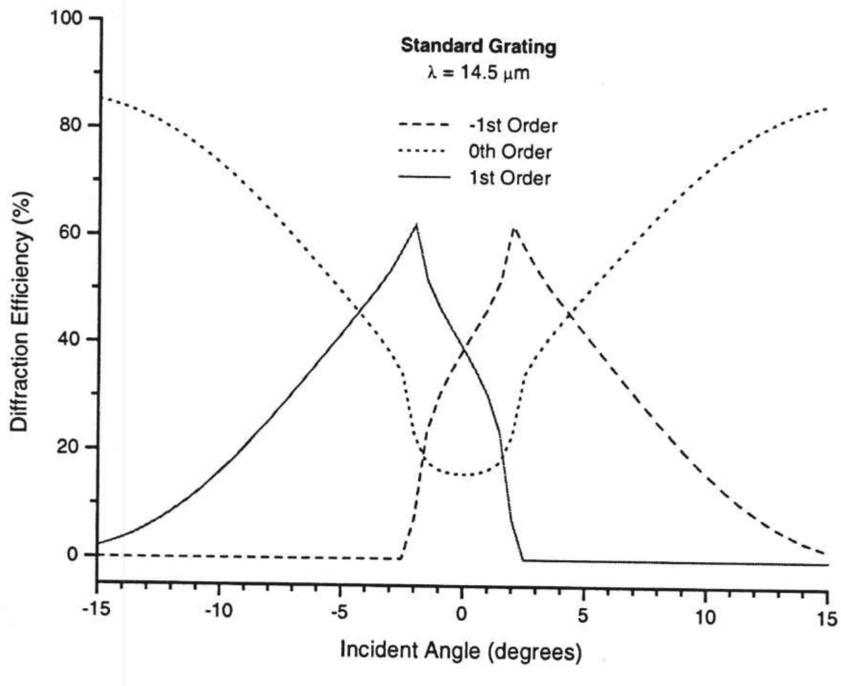
Standard Grating
λ = 14.5 μm
-1st Order
0th Order
1st Order
Diffraction Efficiency (%)
Incident Angle (degrees)
100
80
60
40
20
0
-15
-10
-5
0
5
10
15

(d)

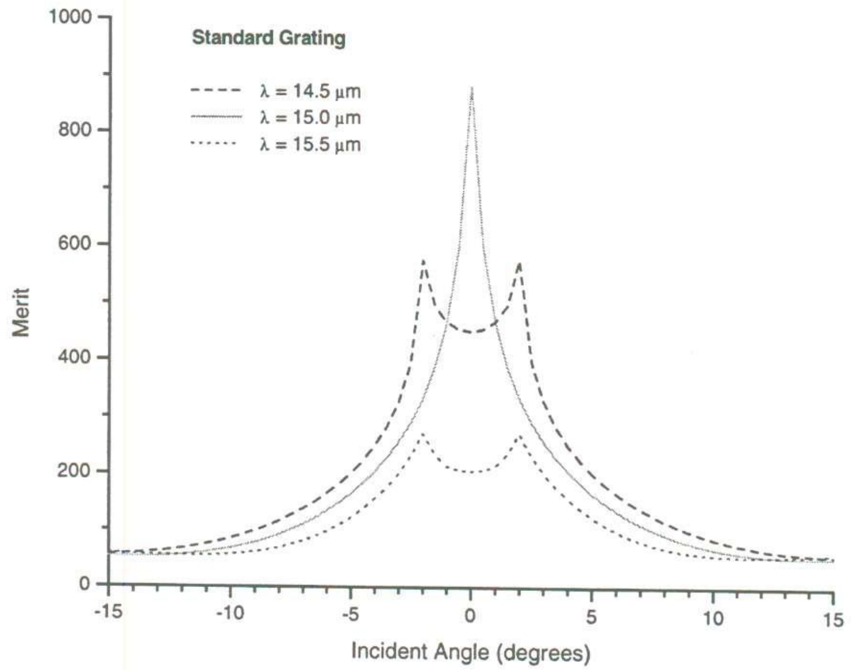

(e)

Figure 9. Angular sensitivity of standard QWIP grating: (a) diffraction angles and (b) efficiencies for λ = 15 μm, (c) diffraction angles and (d) efficiencies for λ = 14.5 μm, (e) field magnitude squared merit function values at λ = 14.5, 15.0, and 15.5 μm.

D. Optimized grating parameters for normal incidence

Because the microlens approach does not look promising, it is important to optimize the grating for normal incidence. This was done by calculating contour plots of the order efficiencies and merit function as a function of grating parameters. Figure 10 shows the merit function as a function of period and fill factor and clearly indicates that the optimum period is 4.85 μm and the optimum fill factor is 0.68. This is rather surprising, since these parameters are identical to the parameters of the standard grating, which was determined from a slice through the standard two-dimensional grating having a period of 4.85 μm and a 2D area fill factor of 46% (fraction of 2D unit cell that is GaAs). Because we are operating in the regime of near unity period to wavelength ratio, it is not expected that a slice through an optimum 2D grating would give an optimum 1D grating. Hence, *it is very likely that the current 2D grating is not optimum and likely has a fill factor that is too small.* What is really needed at this point is an accurate 2D grating solver that could be used to determine the optimum 2D grating parameters.

The other parameter to optimize is the grating depth. Figure 11 shows the merit function as a function of grating depth and fill factor. The optimum fill factor is again 0.68, but the optimum depth is a surprisingly shallow 0.5 μm. This is unexpected because for large period gratings, the optimum depth would be one-quarter of a wavelength or 1.2 μm. This result has been validated both at Georgia Tech and JPL, so it is correct, but it may be some sort of resonance that requires many periods of the grating and may not be experimentally realizable. One feature of the merit function plot (Fig. 10(c)) that should be emphasized is that *if the fill factor of the grating is not correct, then adjusting the depth will not have a large effect.*

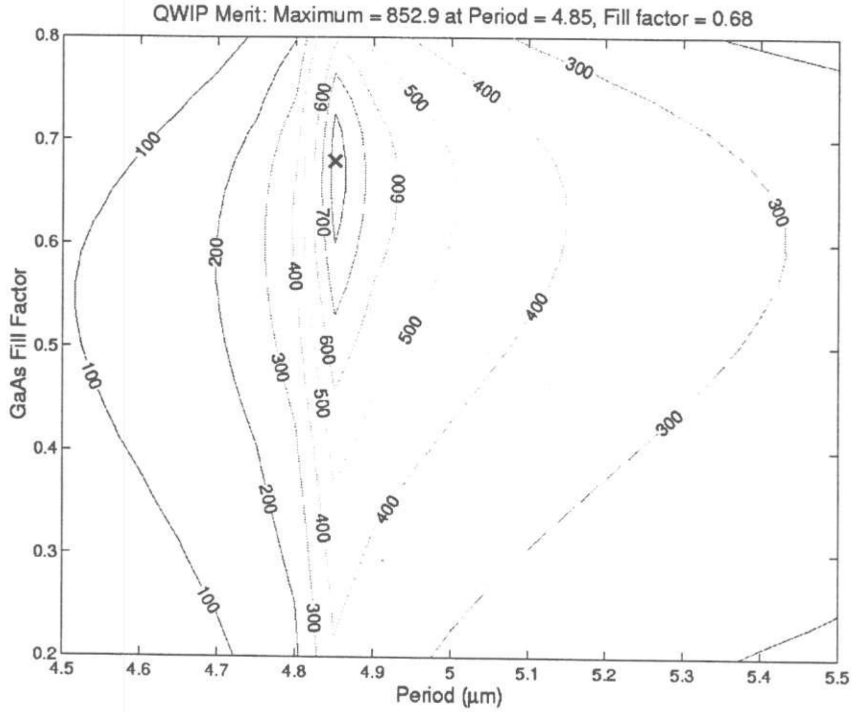

Figure 10. Sensitivity of QWIP optical coupling to grating period and fill factor ($\lambda = 15$ µm).

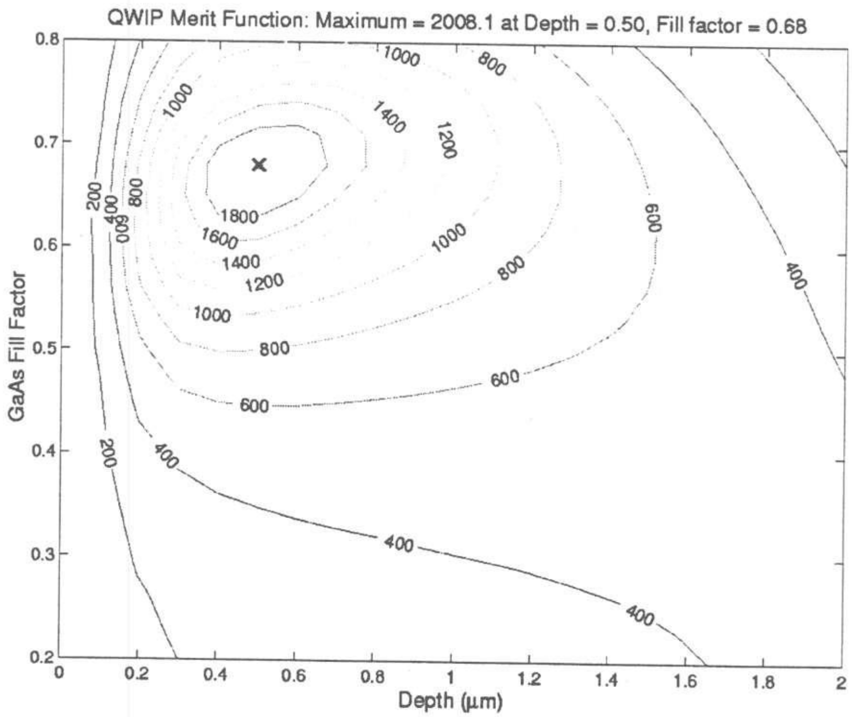

Figure 11. Sensitivity of QWIP optical coupling to grating depth and fill factor ($\lambda = 15$ µm).

E. *Approximate 2D grating simulation*

The optimization simulations shown in Figs. 10 and 11 show that the optimum one-dimensional grating parameters are $\Lambda = 4.85$ µm, F = 68% GaAs, and d = 0.5 µm. The essential question is *what are the optimum parameters for a two-dimensional grating?* RCWA does not work well for 2D *metallic* gratings because too many diffraction orders are required for convergence. Hence it is not feasible to do a rigorous analysis of the 2D metal grating problem. However, RCWA does work well for *dielectric* 2D gratings, and considerable insight can be gained from a 2D dielectric grating analysis. The goal in QWIP grating design is to minimize the reflected zeroth order. If the gold is replaced with high-index dielectric that provides significant reflectivity, the reflected zeroth order diffraction characteristics may be similar to the gold grating. For this study, a dielectric with refractive index of 9.3 was used. For normal incidence on a flat GaAs (n = 3.1) / dielectric (n = 9.3) interface, this gives a substantial reflectance of 25%.

To verify that the dielectric grating behaves similarly to the gold grating, a one-dimensional grating was simulated. A contour plot of the zeroth-order efficiency as functions of depth and fill factor is shown in Fig. 12. The optimum fill factor was determined to be 65%, which is very close to the 68% found for the gold grating. The two-dimensional grating was then simulated. The configuration, looking from the GaAs side, is composed of square GaAs regions surrounded by a grid of grooves filled with dielectric. The 2D simulation results are shown in Fig. 13. The optimum x- and y-fill factors ($F_x = F_y$) are 80% GaAs. Hence the *area* fill factor is 64% GaAs. The current IMAS QWIP grating is being fabricated with $F_x = F_y = 68\%$, or an area fill factor of 46%. It is therefore very likely that the current grating is diffracting a significant fraction of the incident energy into the reflected zeroth order.

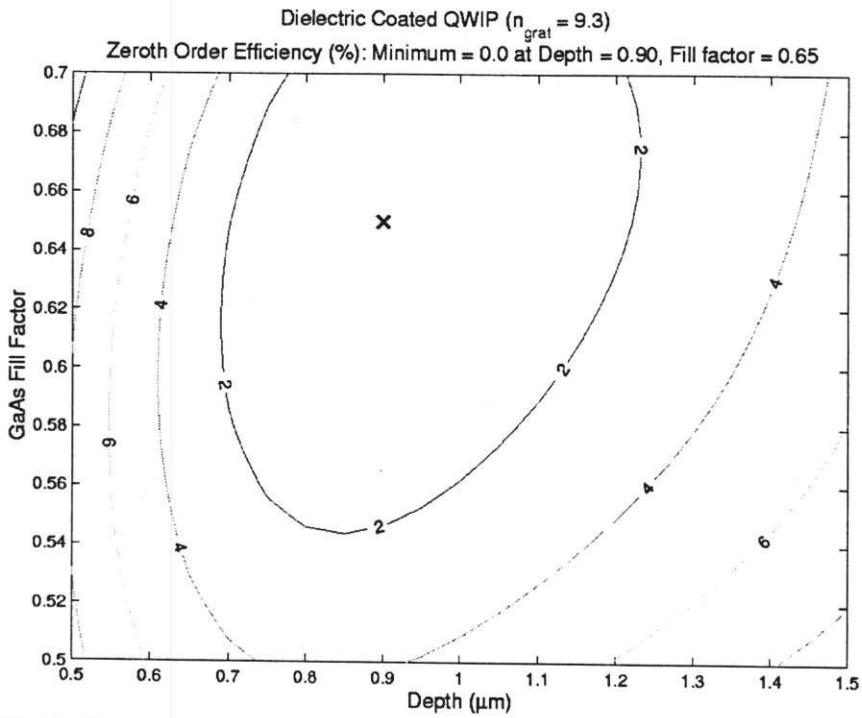

Figure 12. Reflected zeroth order of a *one-dimensional dielectric coated* QWIP grating (λ = 15 μm, Λ = 4.85 μm). Configuration is the same as that shown in Fig. 4, except that the gold is replaced with a dielectric of index 9.3.

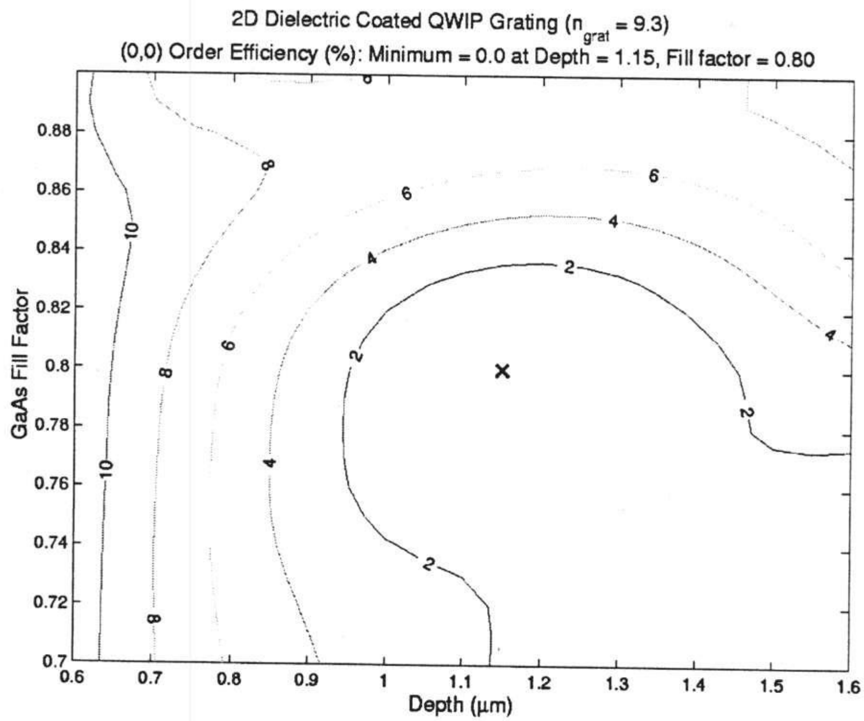

Figure 13. Reflected zeroth order of a *two-dimensional dielectric coated* QWIP grating (λ = 15 μm, $\Lambda_x = \Lambda_y$ = 4.85 μm). Configuration is square GaAs regions surrounded by a grid of grooves filled with dielectric of refractive index 9.3.

V. Finite Gratings

In this section, the boundary element method (BEM) was used to model plane-wave and focused-wave incidence on finite gratings without mesa walls. These simulations indicate the effects of finite number of periods without the complicating effects of mesa sidewalls. For each simulation, the incident field was specified along the GaAs/gold interface, and then the scattered fields on the boundary are determined by the BEM. The field-squared merit function was determined by calculating the total fields inside the quantum well region.

A. Plane wave incidence on a 50 μm-wide grating

In the infinite grating simulations, the sharp peaks near cutoff indicate that some sort of resonance is occurring. These sharp peaks are likely due to waves propagating nearly parallel to the grating. Such waves have long-range interactions with the grating and may not exist in finite-width QWIPs. To study this effect on a reasonably wide, but finite size grating, a plane wave impinging on a 50 μm wide grating was simulated. Figure 14 shows the merit function versus wavelength for two grating depths. Note the lack of a sharp peak in the merit function. It is surprising that the 0.5 μm depth still gives good performance even in this finite-width case. Figure 15 shows the variation of the merit function with grating depth for three different grating periods, Λ = 4.85, 5.00, and 5.25 μm. The optimum depth increases as the grating period increases. This effect is not clearly understood, but in the large Λ/λ limit, the optimum depth should be a $\lambda/4$ = 1.21 μm, so the trend is reasonable. Several single-point simulations of fill factor variation were also performed, and it was determined that 68% GaAs was near optimum, even for this finite-width grating.

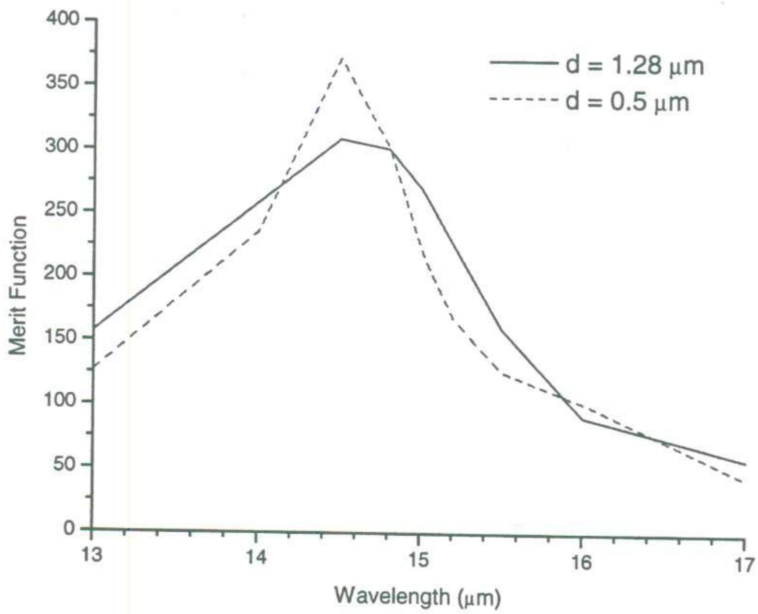

Figure 14. QWIP optical coupling merit as a function of wavelength for a 50 μm wide grating with no mesa. (Λ = 4.85 μm, F = 68%)

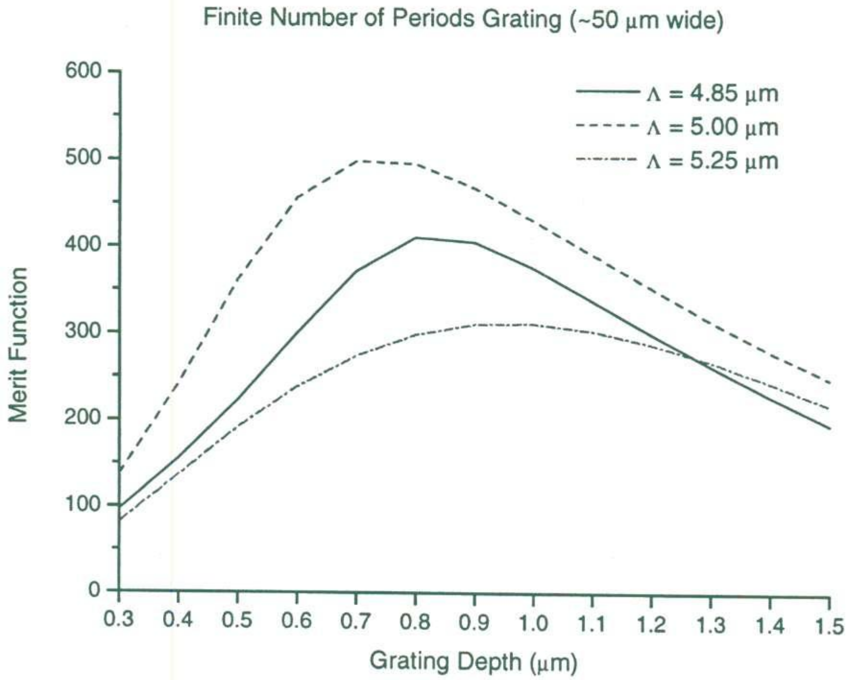

Figure 15. QWIP optical coupling merit as a function of grating depth for a plane wave incident on a 50 micron wide grating with no mesa. (λ = 15 microns, F = 68%).

B. *Focused wave incidence on a 20 μm-wide grating*

One of the main goals of this modeling effort was to determine if a microlens could focus light onto a small QWIP grating and achieve high coupling efficiency. In this simulation, the focused field from an ideal microlens (50 μm wide, 90 μm focal length, 100% efficient) was used as the incident field for a grating having only 4 periods (~20 μm wide). The width of the QW region was equal to the grating width, but because the lens the collection area was the same as for the 50 μm grating, the merit functions from this case and the 50 μm case can be directly compared. Figure 16 shows a plot of the merit function as a function of grating depth. Note that the peak is ~58% of that for plane-wave incidence on the 50 μm mesa. Hence the reduced width grating does not couple all of the focused light into the QWIP. This agrees with the infinite grating simulations.

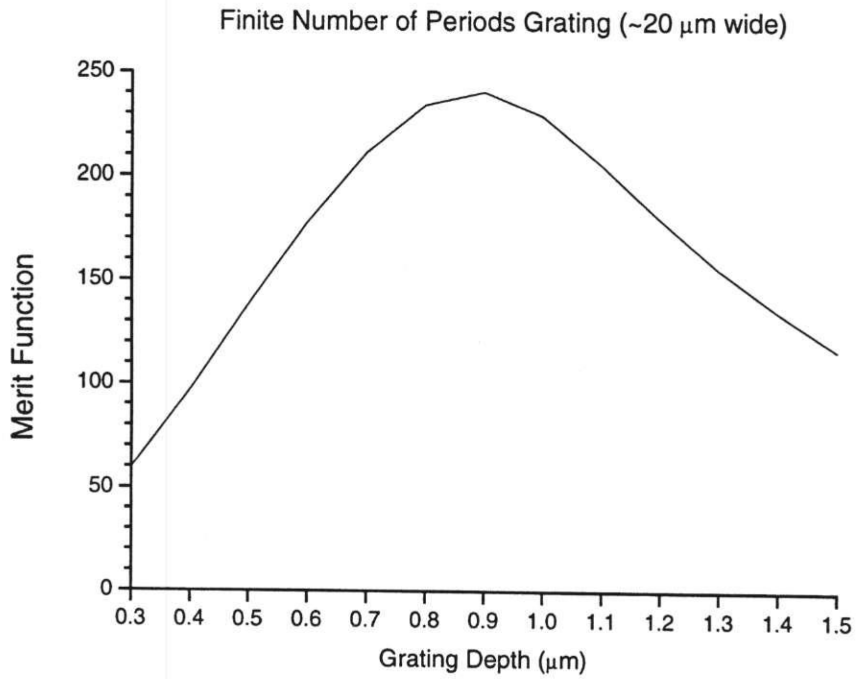

Figure 16. QWIP Merit function versus grating depth for focused wave incident on a 20 micron wide grating with no mesa. (4 periods, $\Lambda = 4.85\ \mu m$, $\lambda = 15\ \mu m$).

VI. Finite Gratings on Mesas

In this section, the finite element method (FEM) was used to model plane waves and focused waves incident on mesas with gratings. For the plane-wave simulations, the mesa was 50 μm wide with a standard grating. For the focused-wave simulation, the incident field was that from a ideal microlens as in Sec. V.B (50 μm wide, 90 μm focal length, 100% efficient) and the mesa was 20 μm wide with a standard grating. Images of the z-polarized field magnitudes are shown in Figs. 17 and 18. The fields inside the 50 micron mesa resemble the fields of the infinite grating (Fig. 5), but with significant disruptions due to the mesa corners. The fields inside the 20 μm mesa do not show vertical interference fringes indicating that that structure is not efficiently diffracting into high-angle waves. The field magnitude squared merit functions are plotted in Figure 19, including the merit function for a 45 degree plane wave incident on a 50 μm mesa with no grating. The merit function peak for the 50 μm grating+mesa compares well with the case without a mesa shown in Fig. 14. The 20 μm grating+mesa coupling is significantly lower than the case without a mesa shown in Fig. 16, indicating that the mesa walls play a larger role as the mesa gets smaller.

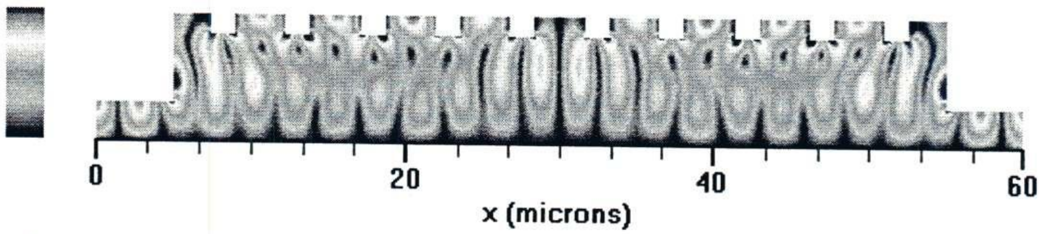

Figure 17. Plot of $|E_z|$ for plane wave incident on 50 micron mesa with standard grating. This plot is flipped vertically compared to previous orientations. The plane wave is incident from bottom.

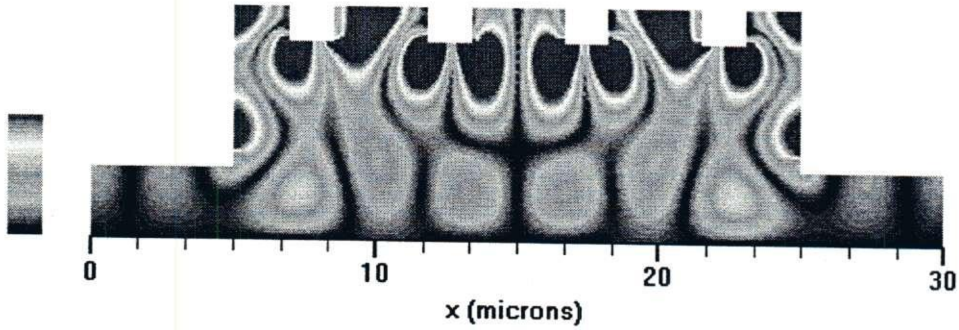

Figure 18. Plot of $|E_z|$ for focused wave incident on 20 micron mesa with standard grating. This plot is flipped vertically compared to previous orientations. The plane wave is incident from the bottom.

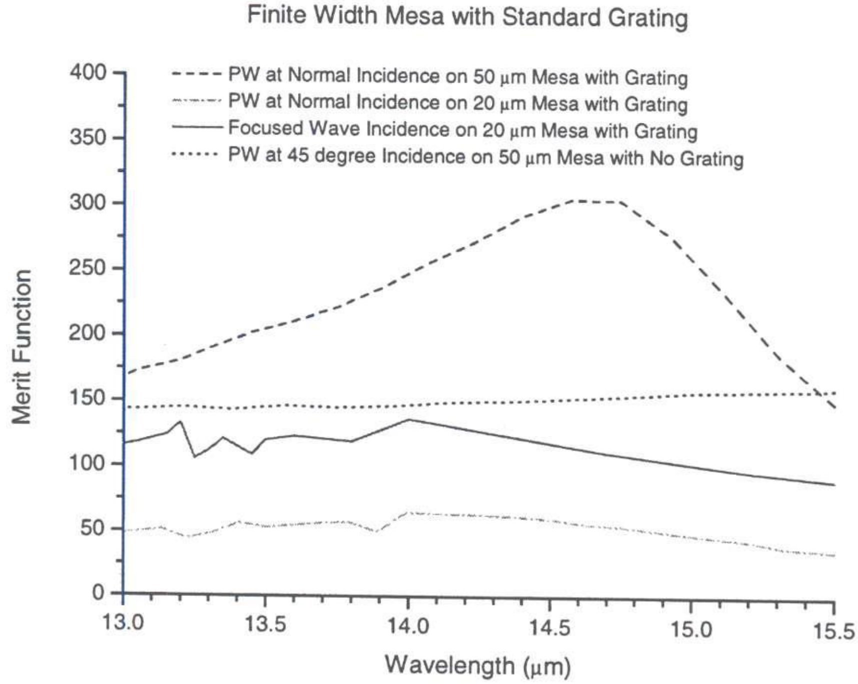

Figure 19. QWIP coupling merit as a function of wavelength for plane-wave and focused radiation incident on mesas of finite width.

VII. Slotted QWIPs

As an alternative to the microlens approach for decreasing the dark current, a novel QWIP structure was invented and termed the "slotted QWIP." The structure is shown in Fig. 20. At first glance it resembles the "enhanced QWIP" developed by Loral, but it differs both structurally and functionally. The key feature that provides dark current reduction is the array of slots that are etched through the QW stack. The slots are filled with air or a low index dielectric, forming a reflective surface around the GaAs QW pillars. This structure was first simulated using a finite-difference (FD) Helmholtz equation solver that is not as accurate as BEM or FEM, but provides similar insight into the fields throughout the structure. By varying the structure parameters (pillar width, slot width, slot index), a resonance was found at which the E_z inside the QW was high. To understand how the structure was working, a single pillar was simulated and the fields were very similar to the periodic case. Hence, a preliminary explanation is that the incident wave sees the GaAs pillar surrounded by low-index dielectric and gets wave-guided in the GaAs pillar. At the end of the pillar, the gold tooth scatters some of the field horizontally. This component of the scattered field reflects back and forth between the walls of the pillar, creating a resonance condition. It is also this component that gets absorbed by the quantum well. Hence it appears that the slotted QWIP does not act as a periodic structure, but rather an array of weakly coupled open-ended cavity resonators.

To accurately model the slotted QWIP structure, it was simulated using RCWA with anisotropic absorption in the QW region. Figure 21 shows the absorption as a function of wavelength for the slotted QWIP. There are several interesting features. First, the shape of the peak is distinctly different from the shape observed for the infinite gratings. It appears more like the shape of a cavity resonance, in agreement with the proposed mode of operation. Second, the peak of the absorption is higher than was achieved with the grating, indicating that perhaps better optical coupling is possible with this structure. This is in addition to the benefit of dark current reduction. The downside of this structure is that fabrication may be difficult due to the small feature sizes, high aspect ratios, and surface leakage current issues.

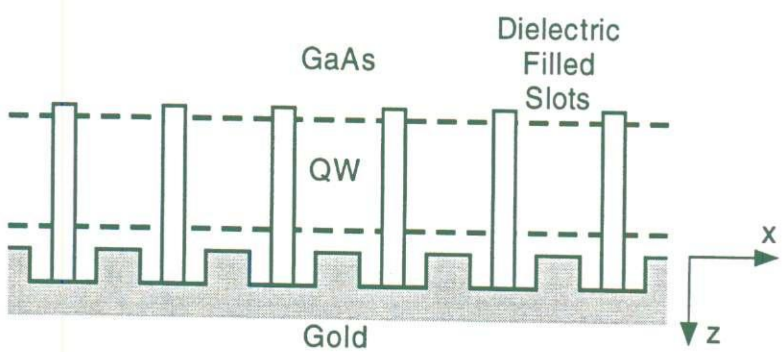

Figure 20. Illustration of slotted QWIP structure

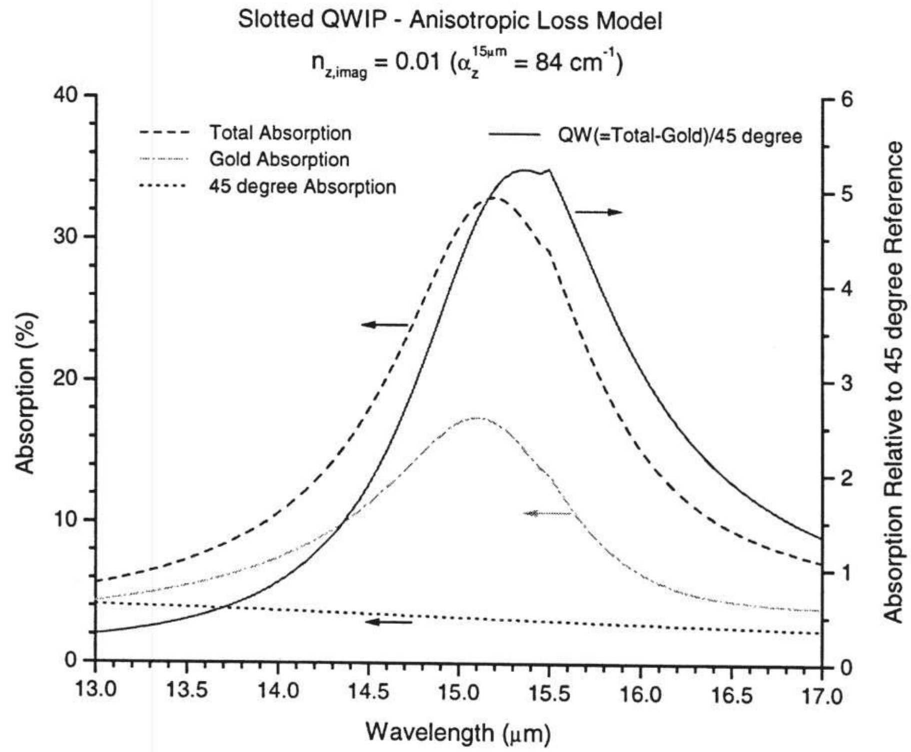

Figure 21. Slotted QWIP performance using anisotropic absorption model. Left axis: percentage of incident power absorbed. Right axis: absorption in QW layers normalized by the absorption of 45 degree incidence on planar GaAs/gold interface. Structure: $\Lambda = 5.00$ μm, slot width = 1.5 μm, slot depth = 4.53 μm (through QW), slot index = 1.0 (air), grating fill factor = 30% gold, grating depth = 1.2 μm.

VIII. Conclusions and Future Work

The simulations described in this report accomplished most of the goals set out in the IMAS modeling program. All three types of grating simulations (infinite, finite, and finite mesa) addressed the question of a microlens focusing to a QWIP grating. For large area gratings, it was determined that the angular selectivity of the grating results in poor lenslet-QWIP coupling. For small gratings on mesas, there may be too few grating periods for efficient coupling and the mesa walls play a significant role. It does not appear possible to significantly improve the focused-light coupling by variation of simple grating parameters such as period, fill factor, and depth. Although the microlens-QWIP simulations yielded negative results, the understanding gained is valuable.

Several positive results came out of this modeling effort. First, the optimization studies of large area gratings indicated that the fill factor should be increased. With the current modeling tools it is not possible to predict how much improvement this will yield, but it is certainly worth experimental investigation. Second, the "slotted QWIP" was proposed as alternative structure for reducing dark current while maintaining optical coupling. While this structure is difficult to fabricate, it is possible with equipment and processing expertise that exists at JPL. The modeling done on the slotted QWIP was very limited, and more simulations of that structure and similar structures should be performed. Finally, several rigorous electromagnetic modeling tools were implemented or improved for this program. For infinite grating analysis, a modular Matlab QWIP grating simulation tool was developed. It can handle arbitrary 1D gratings (including structures having anisotropic absorption) as will as dielectric 2D gratings. If an efficient 2D metallic grating solver is developed, it can be easily incorporated. For finite structures including microlenses, finite-width gratings, and mesas, the boundary element method and the finite element methods were applied to the QWIP problem and flexible simulation tools were developed. The modeling techniques and software developed during this program will continue to enhance further QWIP development at JPL.